



1 Efficient N₂O₅ Uptake and NO₃ Oxidation in the Outflow of Urban Beijing

2 Haichao Wang¹, Keding Lu^{1*}, Song Guo¹, Zhijun Wu¹, Dongjie Shang¹, Zhaofeng Tan¹, Yujue Wang¹,
3 Michael Le Breton², Wenfei Zhu³, Shengrong Lou³, Mingjin Tang⁴, Yusheng Wu¹, Jing Zheng¹, Limin
4 Zeng¹, Mattias Hallquist², Min Hu¹ and Yuanhang Zhang^{1,5}

5

6 ¹State Key Joint Laboratory of Environmental Simulation and Pollution Control, College of
7 Environmental Sciences and Engineering, Peking University, Beijing, China.

8 ²Department of Chemistry and Molecular Biology, University of Gothenburg, Gothenburg, Sweden

9 ³Shanghai Academy of Environmental Sciences, Shanghai, China

10 ⁴State Key Laboratory of Organic Geochemistry and Guangdong Key Laboratory of Environmental
11 Protection and Resources Utilization, Guangzhou Institute of Geochemistry, Chinese Academy of
12 Sciences, Guangzhou, China

13 ⁵CAS Center for Excellence in Regional Atmospheric Environment, Chinese Academy of Sciences,
14 Xiamen, China

15

16 *Corresponding to: Keding Lu (k.lu@pku.edu.cn)

17

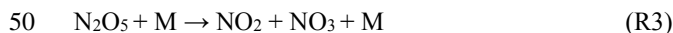
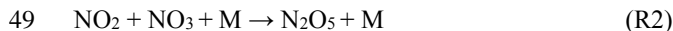
18 **Abstract.** Nocturnal reactive nitrogen compounds are important for understanding regional air
19 pollution. Here we present the measurements of dinitrogen pentoxide (N₂O₅) associated with nitryl
20 chloride (ClNO₂) and particulate nitrate (pNO₃⁻) in a suburban site of Beijing in the summer of 2016.
21 High levels of N₂O₅ and ClNO₂ were observed in the outflow of the urban Beijing air masses, with 1-
22 min average maxima of 937 pptv and 2.9 ppbv, respectively. The N₂O₅ uptake coefficients, γ , and
23 ClNO₂ yield, f , were experimentally determined from the observed parameters. The N₂O₅ uptake
24 coefficient ranged from 0.012 to 0.055, with an average of 0.034 ± 0.018 , which is in the upper range
25 of previous field studies reported in North America and Europe but is a moderate value in the North
26 China Plain (NCP), which reflects efficient N₂O₅ heterogeneous processes in Beijing. The ClNO₂ yield
27 exhibited high variability, with a range of 0.50 to unity and an average of 0.73 ± 0.25 . The nighttime
28 nitrate radical (NO₃) was calculated assuming that the thermal equilibrium between NO₃ and N₂O₅
29 was maintained. In NO_x-rich air masses, the oxidation of nocturnal biogenic volatile organic
30 compounds (BVOCs) was dominated by NO₃ rather than O₃. The production rate of organic nitrates
31 (ONs) via NO₃+BVOCs was significant, with an average of 0.11 ± 0.09 ppbv h⁻¹. We highlight the
32 importance of NO₃ oxidation of VOCs in the formation of ONs and subsequent secondary organic
33 aerosols in summer in Beijing. The capacities of BVOCs oxidation and ONs formation are maximized
34 and independent of NO_x under a high NO_x/BVOCs ratio condition (>10), which indicates that the
35 initial reduction of the NO_x emission cannot help reduce the nocturnal formation of ONs.

36



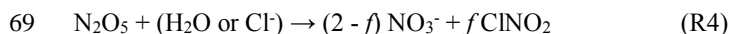
37 1. Introduction

38 It has been well recognized that reactive nitrogen compounds, specifically the nitrate radical (NO_3)
39 and dinitrogen pentoxide (N_2O_5), play a key role in nighttime chemistry (Wayne et al., 1991; Brown
40 and Stutz, 2012). NO_3 is the most important oxidant in the nighttime and can be considered the
41 nighttime analogue of the hydroxyl radical (OH) for certain VOCs (Wayne et al., 1991; Benton et al.,
42 2010). NO_3 can initiate the removal processing of many kind of anthropogenic and biogenic emissions
43 after sunset. In the NO_x -rich plumes, NO_3 is responsible for the vast majority of the oxidation of
44 biogenic VOCs because of its rapid reactions with unsaturated hydrocarbons (Edwards et al., 2017).
45 NO_3 is predominantly formed by the reaction of NO_2 with O_3 (R1) and further reacts with NO_2 to
46 produce N_2O_5 (R2). Because N_2O_5 is rapidly decomposed back into NO_2 and NO_3 (R3), NO_3 and N_2O_5
47 are in dynamic equilibrium in the troposphere.



51 Photolysis of NO_3 and its reaction with NO are rapid, which leads to a daytime NO_3 lifetime being
52 shorter than 5 s with extremely low concentrations, whereas in low-NO air masses, the fate of NO_3 is
53 mainly controlled by the mixing ratios of various VOCs and N_2O_5 heterogeneous hydrolysis because
54 the two terms are the dominating loss pathways of NO_3 and N_2O_5 . The VOCs reaction is significant
55 downwind of a human-dominated area or a strongly urban-influenced forested area in summer. The
56 NO_3 oxidation of VOCs was responsible for more than 70% nocturnal NO_3 loss in Houston (Stutz et
57 al., 2010) and contributed approximately 50% in the forest region in Germany (Geyer et al., 2001).
58 The reactions of NO_3 with several BVOCs produce considerable organic nitrates (ONs) with efficient
59 yields, which act as important precursors of secondary organic aerosols (SOA). The reaction of NO_3
60 with isoprene has a considerable SOA yield of 23.8% (Ng et al., 2008), and the reaction with
61 monoterpenes, such as limonene, can reach 174% at ambient temperatures (Boyd et al., 2017). The
62 reactions of $\text{NO}_3 + \text{BVOCs}$ are critical to the studies of aerosols on regional and global scales (Fry et
63 al., 2009; Rollins et al., 2009; Pye et al., 2010; Ng et al., 2017). For example, ONs had extensive
64 percentages of fine particulate nitrate (pNO_3^-) (34% - 44%) in Europe (Kiendler-Scharr et al., 2016).

65 The heterogeneous hydrolysis of N_2O_5 produces soluble nitrate (HNO_3 or NO_3^-) and nitryl chloride
66 (ClNO_2) on the chloride-containing aerosols (R4) (Finlayson-Pitts et al., 1989). This reaction is known
67 to be an important intermediate in the NO_x removal processes (Brown et al., 2006). The rate coefficient
68 of the heterogeneous N_2O_5 reaction is given in Eq. 1 (Tang et al., 2017).



70 $k_{\text{N}_2\text{O}_5} = 0.25 \cdot c \cdot \gamma(\text{N}_2\text{O}_5) \cdot S_a$ (Eq. 1)

71 where c is the mean molecule speed of N_2O_5 , S_a is the aerosol surface concentration and $\gamma(\text{N}_2\text{O}_5)$ is the
72 N_2O_5 uptake coefficient. N_2O_5 heterogeneous hydrolysis is one of the major uncertainties of the NO_3
73 budget since the N_2O_5 uptake coefficient can be highly variable and difficult to quantify (Brown and
74 Stutz, 2012; Chang et al., 2011; H. C. Wang et al., 2016). Laboratory and field measurement studies
75 have reported that the N_2O_5 uptake coefficient has large variability and ranges from <0.001 to 0.1; the



76 N₂O₅ uptake coefficient is subject to relative humidity (RH), particle morphology, compositions (water
77 content, nitrate, sulfate, organic or mineral particles) and other factors (e.g., Wahner et al., 1998;
78 Mentel et al., 1999; Hallquist et al., 2003; Thornton et al., 2003; Thornton et al., 2005; Brown et al.,
79 2006; Bertram and Thornton, 2009; Tang et al., 2012, 2014; Gaston et al., 2014; Grzinic et al., 2015).
80 The coupled chemical mechanisms in ambient conditions are still not well understood. ClNO₂ forms
81 and accumulates with a negligible sink during the night and further photolyses and liberates the
82 chlorine radical (Cl) and NO₂ after sunset. Hundreds of pptv to ppbv of ClNO₂ can lead to several
83 ppbv of O₃ enhancement and significant primary ROx production (Osthoff et al., 2008; Thornton et al.,
84 2010; McLaren et al., 2010; Riedel et al., 2014; Sarwar et al., 2014; Tham et al., 2016).

85 Large amounts of NOx have been emitted for the past several decades in China, but comprehensive
86 field studies of the nighttime chemical processes of reactive nitrogen oxides remain sparse. Previous
87 studies have found high mixing ratios of NO₃ associated with high NO₃ reactivity in the megacities in
88 China, including Shanghai, the Pearl River Delta (PRD) and Beijing (Li et al., 2012; Wang et al., 2013;
89 Wang et al., 2015). N₂O₅ concentration was elevated in Beijing (H. C. Wang et al., 2017a; H. C. Wang
90 et al., 2017c) but was moderate in other places of North China Plain (NCP), such as Wangdu, Jinan
91 and Mount Tai (Tham et al., 2016; X. F. Wang et al., 2017; Z. Wang et al., 2017). Recently, the N₂O₅
92 uptake coefficients were determined to be very high, even up to 0.1 in NCP, but the reason is still not
93 well studied (H. C. Wang et al., 2017c; X. F. Wang et al., 2017; Z. Wang et al., 2017). Reactive N₂O₅
94 chemistry was also reported in Hong Kong, which had the highest N₂O₅ concentration (T. Wang et al.,
95 2016; Brown et al., 2016). Observations and model simulations revealed that fast heterogeneous uptake
96 of N₂O₅ is an important pathway of pNO₃⁻ formation in China (H. C. Wang et al., 2017b; H. C. Wang
97 et al., 2017c; Z. Wang et al., 2017; Su et al., 2017); the reaction also considerably contributed to NOx
98 removal (Z. Wang et al., 2017; Brown et al., 2016). Moreover, chlorine activation from N₂O₅ uptake
99 had a significant effect on daytime photolysis chemistry in China (Xue et al., 2015; Li et al., 2016;
100 Tham et al., 2016; T. Wang et al., 2016).

101 In this study, to quantify the contribution of NO₃ and N₂O₅ chemistry to the atmospheric oxidation
102 capacity and the NOx removal process in the outflow of urban Beijing, we reported the measurement
103 of N₂O₅, ClNO₂, and related species in the surface layer of a suburban site in Beijing and determined
104 the N₂O₅ heterogeneous uptake coefficients and ClNO₂ yields. The nighttime NO₃ oxidation to the
105 biogenic VOCs and its impact on the ONs formation in the NOx-rich region were diagnosed. Finally,
106 the nighttime NOx removal via the NO₃ and N₂O₅ chemistry was estimated and discussed.

107

108 **2. Method**

109 **2.1 The site**

110 Within the framework of a Sino-Sweden joint research project, “Photochemical Smog in China”, a
111 summer field campaign was conducted in Beijing to enhance our understanding of the secondary
112 chemistry via photochemical smog and the heterogeneous reactions (Hallquist et al., 2016). The data
113 presented here were collected at a regional site, PKU-CP (Peking University Changping campus), from
114 23 May to 5 June 2016. The measurement site is located in the northern rural area of Beijing,



115 approximately 45 km from the city center; the closest road is approximately 1 km to the south, and
116 there are no major industry surroundings (Figure 1). The site is surrounded to the north, east and west
117 by mountains. The general feature of this site is that it captures air masses with strong influences from
118 both urban and biogenic emissions. Instruments were set up on the fifth floor of the main building of
119 the campus with inlets approximately 12 m above the ground. Time is given in this paper as CNST
120 (Chinese National Standard Time = UTC+8 h). During the campaign, sunrise was at 05:00 CNST and
121 sunset was at 19:30 CNST.

122 **2.2 Instrument setup**

123 A comprehensive suite of trace gas compounds and aerosol properties was measured in the field study,
124 and the details are listed in Table 1. N_2O_5 was measured by a newly developed cavity enhanced
125 absorption spectrometer (CEAS; H. C. Wang et al., 2017a). In the CEAS, ambient N_2O_5 was thermally
126 decomposed to NO_3 in a perfluoroalkoxy alkanes (PFA) tube (length: 35 cm, I.D.: 4.35 mm) heated to
127 120 °C and was then detected within a PFA resonator cavity; the cavity was heated to 80 °C to prevent
128 NO_3 reacting back to N_2O_5 . Ambient gas was sampled with a 1.5-m sampling line (I.D.: 4.35 mm) with
129 a flow rate of 2.0 L min⁻¹. NO was injected for 20 seconds to destroy NO_3 from N_2O_5 thermal
130 decomposition in a 5-minute cycle, and the corresponding measurements were then used as reference
131 spectra (I_0). A Teflon polytetrafluoroethylene (PTFE) filter was used in the front of the sampling
132 module to remove ambient aerosol particles. The filter was replaced with a fresh one every hour to
133 avoid the decrease of N_2O_5 transmission efficiency due to aerosol accumulation on the filter. The limit
134 of detection (LOD) was 2.7 pptv (1 σ), and the measurement uncertainty was 19%.

135 ClNO_2 and N_2O_5 were also detected using a Time of Flight Chemical Ionization Mass Spectrometer
136 (ToF-CIMS) with the Filter Inlet for Gas and AEROSols (FIGAERO; Lopez-Hilfiker et al., 2014;
137 Bannan et al., 2015). Briefly, the gas phase species were measured via a 2-m-long, 6-mm-outer-
138 diameter PFA inlet while the particles were simultaneously collected on a Teflon filter via a separate
139 2-m-long, 10-mm-outer-diameter copper tubing inlet; both had flow rates of 2 L min⁻¹. The gas phase
140 was measured for 25 minutes at 1 Hz, and the FIGAERO instrument was then switched to place the
141 filter in front of the ion molecule region; it was then heated incrementally to 200 °C to desorb all the
142 mass from the filter to be measured in the gas phase, which resulted in high-resolution thermo grams.
143 Formic acid calibrations were performed daily using a permeation source maintained at 40 °C. Post-
144 campaign laboratory calibrations of N_2O_5 were first normalized to the campaign formic acid
145 calibrations to account for any change in sensitivity (Le Breton et al., 2014). Then, ClNO_2
146 measurements were quantified by passing the N_2O_5 over a wetted NaCl bed to produce ClNO_2 . The
147 decrease in N_2O_5 from the reaction with NaCl was assumed to be equal to the concentration of ClNO_2
148 produced (i.e., 100% yield). The sensitivities of the CIMS to N_2O_5 and ClNO_2 were found to be 9.5
149 and 1.2 ion counts per pptv Hz⁻¹, respectively, with errors of 23% and 25% for ClNO_2 and N_2O_5 ,
150 respectively. The limit of detection (LOD) for ClNO_2 and N_2O_5 were 16 and 8 pptv, respectively. An
151 intercomparison of N_2O_5 measurements between the CEAS and FIGAERO-ToF-CIMS showed good
152 agreement; a companion paper on chlorine photochemical activation during this campaign gives
153 detailed intercomparison results of N_2O_5 measured by the two different techniques (Le Breton et al.,
154 2018).



155 Sub-micron aerosol compositions (PM_{1.0}), including nitrate, sulfate, chloride, ammonium and
156 organic compounds, were measured by a High Resolution Time of Flight Aerosol Mass Spectrometer
157 (HR-ToF-AMS) (DeCarlo et al, 2006, Zheng et al., 2017). Particle number and size distribution (PNSD)
158 was measured by a scanning mobility particle sizer (SMPS, TSI 3936) and an aerosol particle sizer
159 (APS, TSI 3321) (Yue et al., 2009). SMPS measured the particles in the range between 3.5 nm and
160 523.3 nm in diameter, and APS measured the particles with a diameter range from 597.6 nm to 10.0
161 μm . S_a was calculated based on the dry-state particle number and geometric diameter in each size bin
162 (3.5 nm - 2.5 μm). Dry-state S_a was corrected to wet particle-state S_a for particle hygroscopicity by a
163 growth factor. The growth factor, $f(\text{RH})=1 + 8.77 \times (\text{RH}/100)^{9.74}$, was derived from the aerosol optical
164 property in autumn in Beijing and is valid for 30% < RH < 90% (Liu et al., 2013). The uncertainty of
165 the wet aerosol surface areas was estimated to be ~30%, associated from the error from dry PNSD
166 measurement (~20%) and the growth factor (~20%). During this measurement, fine particles below
167 500 nm contributed to more than 90% of the total particle aerosol surface area.

168 VOCs were measured by Proton Transfer Reaction Mass Spectrometry (PTR-MS) with a time
169 resolution of 5 minutes (de Gouw and Warneke et al., 2007; Wang et al., 2014). A commercial
170 instrument (Thermo Electron model 42i) equipped with a molybdenum-catalytic converter was used
171 to monitor NO_x. The LOD were 60 pptv (1 min) for NO and 300 pptv (1 min) for NO₂, with both at a
172 20% precision (Tan et al., 2017). The molybdenum-catalytic technique not only converts NO₂ to NO
173 but also converts ambient NO_y such as peroxyacetyl nitrate (PAN) and HNO₃. Therefore, the measured
174 NO₂ concentration corresponded to NO₂ + NO_y and was normally higher than the real concentration,
175 especially in an aged air mass with high NO_x conditions. In this study, we used a factor of 0.6 to correct
176 the nighttime NO₂ concentration (a detailed explanation is in the Support Information Text S1 and
177 Figure S1). O₃ was measured by a commercial instrument using ultraviolet (UV) absorption (Thermo
178 Electron model 49i); the LOD was 0.5 ppbv, with an uncertainty of 5%. The mass concentration of
179 PM_{2.5} was measured using a standard Tapered Element Oscillating Microbalance (TEOM, 1400A
180 analyzer). Meteorological parameters included relative humidity, temperature, pressure, wind speed,
181 and wind direction and were available during the campaign. Photolysis frequencies were calculated
182 from the spectral actinic photon flux density measured by a spectroradiometer (Bohn et al., 2008).

183

184 3. Results

185 3.1 Overview

186 During the campaign, the meteorological conditions of the site were characterized by high temperature
187 and low relative humidity (RH); the temperature ranged from 10 - 34 °C and was 23 ± 5 °C on average,
188 and RH ranged from 10% - 80%, with an average of $37\% \pm 15\%$. Because of the special terrain of the
189 observation site, the local wind was measured by the in situ meteorological stations; the site has a
190 typical mountain-valley breeze that cannot reflect the general air mass movement patterns at slightly
191 higher altitudes. Figure 2 shows the calculated backward trajectories using the Hybrid Single-Particle
192 Lagrangian Integrated Trajectory (HYSPLIT) model (Draxler and Rolph, 2003); these images show
193 the 24-h backward particle dispersion trajectories for 12:00 local time (CNST) as the starting time
194 during May 23 - July 5, 2016. According to the results of HYSPLIT, the arrivals of air masses were



195 mainly from the northwest and the south. Therefore, we meteorologically separated the measurement
196 period into two parts. The first three days show that the air masses came from the north or northwest;
197 the air masses represent the background region (defined as Background Air Mass, BAM). The air
198 masses after May 26 originated from the polluted NCP and passed over urban Beijing; they were
199 characterized by large NO_x emissions and severe photochemical pollution (defined as Urban Air Mass,
200 UAM).

201 The time series of N₂O₅, ClNO₂ and other relevant species are shown in Figure 3, and nighttime
202 statistical results are listed in Table S1. The daily 8-h maximum of O₃ concentration exceeded 93 ppbv
203 (Chinese national air quality standard) for 8 of 12 days, and all the O₃-polluted air masses came from
204 the urban region. When the air masses were from the background region, the daily maximum of O₃
205 was only approximately 60 ppbv, much lower than that from the urban region. The NO₂ concentration
206 was elevated, with a nocturnal average value over 10 ppbv during the urban air mass period. The
207 nocturnal nitrate radical production rate, P(NO₃), was profound, with an average of 1.2 ± 0.9 ppbv h⁻¹,
208 which is comparable with rates previously reported in the NCP and Hong Kong (Tham et al., 2016;
209 Brown et al., 2016; Z. Wang et al., 2017; X. F. Wang et al., 2017). The daily peaks of N₂O₅ were 100-
210 500 pptv most nights; the maximum of 937 pptv in a 1-min average was observed near 20:00 on the
211 early night of June 2, when the P(NO₃) was up to 4 ppbv h⁻¹. The average mixing ratio of N₂O₅ was 73 ± 90 pptv,
212 which is much higher than recent measurements reported in North China (Tham et al., 2016;
213 X. F. Wang et al., 2017; Z. Wang et al., 2017) but much lower than that observed in the residual layer
214 of the outflow from the PRD region, where the N₂O₅ was up to 7.7 ppbv (T. Wang et al., 2016). With
215 an elevated O₃ mixing ratio in the first half of the night, the NO lifetime was only several minutes, and
216 the mixing ratio of NO concentration was observed below the detection limit. During the second half
217 of the night when the O₃ concentration was consumed to low concentration, high levels of NO could
218 occasionally be observed, and N₂O₅ dropped to zero because of the fast titration by NO, such as the
219 events that occurred on the second half of the nights of May 24, 28, 30. The PM_{2.5} mass concentration
220 was moderate during the measurement period, with an average of 26 ± 21 $\mu\text{g m}^{-3}$, and the average
221 aerosol surface area was $560 \pm 340 \mu\text{m}^2 \text{cm}^{-3}$. Elevated ClNO₂ was observed to have a daily maximum
222 1-min average of over 800 pptv during the urban air masses period; the campaign maximum of up to
223 2.9 ppbv was observed on the morning (05:30) of May 31, which implied that fast N₂O₅ heterogeneous
224 hydrolysis and effective ClNO₂ yields are common in Beijing. The level of ClNO₂ was comparable
225 with the results in NCP (Tham et al., 2016; X. Wang et al., 2017; Z. Wang et al., 2017) but slightly
226 higher than that measured in coastal (e.g., Osthoff et al., 2008) and inland sites (e.g., Thornton et al.,
227 2010) in other regions of the world.

228 3.2 Mean diurnal profiles

229 The mean diurnal profiles of the measured NO₂, O₃, N₂O₅, ClNO₂ and the particle chloride content are
230 shown in Figure 4, as well as the calculated NO₃ based on the thermal equilibrium of NO₂, NO₃ and
231 N₂O₅. The left panels show the average results of the BAM period, and the right panels show those of
232 the UAM period. The NO₂ and O₃ from the UAM were much higher than were those from the BAM,
233 as were the mixing ratios of N₂O₅, NO₃ and ClNO₂. The daily variation tendencies of those species in
234 the two kinds of air masses were similar. N₂O₅ began to accumulate in the late afternoon and increased
235 sharply after sunset. The single peak occurred near 20:00 and then gradually decreased to the LOD



236 before sunrise; the N_2O_5 maxima occurred at a similar time to our previous observation in urban
237 Beijing (H. C. Wang et al., 2017c); however, the N_2O_5 decrease rate after the peak time was much
238 slower than that in urban Beijing, where the N_2O_5 dropped to almost zero in 2-4 hours, which suggests
239 a relatively slow N_2O_5 loss rate in suburban Beijing. The peaks of N_2O_5 during the BAM period and
240 the UAM period were approximately 75 pptv and 150 pptv, respectively. The calculated NO_3 diurnal
241 profile was quite similar to that of N_2O_5 , and the peaks of NO_3 during the BAM and UAM periods
242 were approximately 11 pptv and 27 pptv, respectively.

243 ClNO_2 accumulated corresponding to N_2O_5 after sunset but ClNO_2 peaked in the middle or the
244 second half of the night since the nocturnal sinks of ClNO_2 were negligible to our knowledge. The
245 diurnal peak of ClNO_2 in the BAM period was approximately 125 pptv, whereas the diurnal peak of
246 ClNO_2 was over 780 pptv in the UAM period and approximately 6 times as high as that in the UAM
247 period. Particle chloride (Cl^-) is regarded as a key factor that affected the ClNO_2 yield on the aerosol
248 surface. Higher particle chloride led to higher ClNO_2 yield and promoted the N_2O_5 conversion to
249 ClNO_2 (e.g., Roberts et al., 2009), whereas the particle chloride content during the measurement was
250 below 60 pptv and was extremely lower than the mixing ratio of ClNO_2 . The HYSPLIT model results
251 showed that the air masses had almost always continental conditions; as was mentioned above, fine
252 particles dominated the S_a , which meant that large amounts of the particle chloride were not
253 replenished by NaCl from marine sources but possibly by the gas-phase HCl (Ye et al., 2016). Cl^- was
254 found to be correlated strongly with CO and SO_2 , likely to originate from an anthropogenic source,
255 such as power plants or combustion sources (Le Breton et al., 2018). Up to 10 ppbv of HCl was
256 observed by a Gas and Aerosol Collector combined with Ion Chromatography (GAC-IC; Dong et al.,
257 2012) in the urban Beijing in September, 2016, which implies that the potential particle Cl source was
258 sufficient and the gas-phase HCl was possibly the main particle chloride source by the acid
259 replacement reaction. After sunrise, ClNO_2 was photolyzed and decreased with the increasing
260 photolysis intensity; however, the photolysis with profound ClNO_2 was still maintained until noon.
261 Similar to the studies reported in London, Texas and Wangdu (Bannan et al., 2015; Faxon et al., 2015;
262 Tham et al., 2016), we observed sustained elevated ClNO_2 events after sunrise in 5 of 12 days. For
263 example, on the morning of May 30, ClNO_2 increased after sunrise and peaked at approximately 8:00
264 am, with a concentration over 500 pptv, which was impossible from the local chemical formation since
265 N_2O_5 dropped to almost zero and the needed N_2O_5 uptake coefficients were unrealistically high.
266 Previous work has suggested that abundant ClNO_2 produced in the residual layer at night and
267 downward transportation in the morning may help to explain this phenomenon (Tham et al., 2016).

268 3.3 Variation of N_2O_5 in the background air masses

269 During the BAM period, the O_3 concentration was excessive compared with NO_2 . In the NO_3 and N_2O_5
270 formation processes, the limited NO_2 in high O_3 region indicates that the variation of NO_2 is more
271 essential to the variation of the N_2O_5 concentration. As shown in Figure 5, during the night of May 24
272 (20:00 - 04:00), the local emission of NO was negligible. O_3 concentration was larger than 25 ppbv,
273 much higher than NO_2 and free of the local NO emission. The variation of N_2O_5 concentration was
274 highly correlated with the mixing ratio of NO_2 ($R^2 = 0.81$). The result suggests that when the air mass
275 with high O_3 was sampled from the background air mass, the N_2O_5 concentration was especially
276 subjected to the NO_2 concentration rather than O_3 . Furthermore, The variation of N_2O_5 concentration



277 was considerably correlated with the NO_3 production rate ($R^2 = 0.60$), suggests the mixing ratio of
278 N_2O_5 was subject to the formation processes in clean air masses.

279 **3.4 Elevated ClNO_2 to N_2O_5 ratio**

280 Large day-to-day variabilities of N_2O_5 and ClNO_2 were observed during the measurement period.
281 Following the work of Osthoff et al. (2008), Mielke et al. (2013), Phillips et al. (2012) and Bannan et
282 al. (2015), we used the relative production rates, $\text{ClNO}_2:\text{N}_2\text{O}_5$, to describe the conversion capacity of
283 N_2O_5 to ClNO_2 . The nighttime peak values and mean values were used to calculate the ratios, and two
284 kinds of daily ratios are listed in Table S2. The average nighttime ratio ranged from 0.7 to 42.0, with
285 a mean of 7.7 and a median of 6.0. The ClNO_2 formation was effective, with $\text{ClNO}_2:\text{N}_2\text{O}_5$ ratios larger
286 than 1:1 throughout the campaign, except for the night of May 26, when the ratio was 0.7:1. Previous
287 observations of the $\text{ClNO}_2:\text{N}_2\text{O}_5$ ratios are summarized in Table 2. Compared with the results
288 conducted in similar continental regions in European and America (0.2 - 3.0), the ratios in this work
289 were significantly higher and consistent with the recent studies in the NCP, which suggests that high
290 $\text{ClNO}_2:\text{N}_2\text{O}_5$ ratios were ubiquitous in the NCP and implies that the ClNO_2 yield via N_2O_5 uptake is
291 effective.

292

293 **4. Discussion**

294 **4.1 Determination of N_2O_5 uptake coefficients**

295 A composite term, $\gamma \times f$, was used to evaluate the overall ClNO_2 yield from N_2O_5 heterogeneous
296 hydrolysis (Mielke et al., 2013); the term was estimated by considering the production rate of ClNO_2
297 and using the measured N_2O_5 and S_a . The values calculated based on the field observations are listed
298 in Table S3 and had moderate variability, a range from 0.008 - 0.035 and an average of 0.019 ± 0.009 .
299 Table 3 summarizes the $\gamma \times f$ values derived in the previous field observations. The value in suburban
300 Germany was between 0.001 and 0.09, with the average of 0.014 (Phillips et al., 2016), and the average
301 value in Mt. Tai, China, was approximately 0.016 (X. F. Wang et al., 2017). Therefore, the average
302 value in this study was comparable with that of the two suburban sites, whereas in an urban site of
303 Jinan, China, the value was lower than 0.008 and comparable with that in the CalNex-LA campaign.
304 The three sets of $\gamma \times f$ values from suburban regions were approximately twice as large as those in
305 urban regions, which implies that the composited ClNO_2 yields in the aged air masses in suburban
306 regions were more efficient than in the urban region. The difference of the overall yield between the
307 two regions may have been caused by (1) the particle morphology variation because of particle aging,
308 such as the particle mixing state, O:C ratio, particle viscosity and solubility (Riemer et al., 2009;
309 Gaston et al., 2014; Grznic et al., 2015) or (2) the particle compound variation such as the liquid water
310 content and the Cl^- content. The liquid water content and the Cl^- content were proposed to affect the
311 ClNO_2 yield because those particle physicochemical properties were reported to affect the N_2O_5 uptake
312 coefficient (Bertram and Thornton, 2009).



313 According to the R4 reaction, pNO_3^- and ClNO_2 were formed by N_2O_5 heterogeneous uptake, with
314 yields of $2 - f$ and f , respectively. Following the recent work of Phillips et al., (2016), we used the
315 observed pNO_3^- and ClNO_2 formation rates to derive individual γ and f . The calculations assumed that
316 the relevant properties of the air mass are conserved and that the losses of produced species are
317 negligible; additionally, the N_2O_5 uptake coefficients and the ClNO_2 yield are independent of particle
318 size. The nights characterized by the following two features were chosen for further analysis: (1) A
319 clear covariance existed between the pNO_3^- and ClNO_2 , which indicated that pNO_3^- and ClNO_2 were
320 to some extent predominantly produced by N_2O_5 uptake, and the HNO_3 uptake was not important for
321 pNO_3^- formation. (2) An equivalent or increase in ammonium was accompanied by an increase of
322 pNO_3^- , which suggested that the gas-phase ammonia was repartitioned to form ammonium nitrate and
323 suppress the release of HNO_3 . The rich-ammonia conditions in Beijing (Liu et al., 2017) demonstrated
324 that the degassing of HNO_3 at night can be effectively buffered by the high concentrations of ammonia
325 presented in the NCP. During this campaign, five nights were eligible for the following analysis. Three
326 different types of derivation were proposed by Phillips et al., (2016), based on the observational data
327 of N_2O_5 , ClNO_2 , pNO_3^- and S_a ; the most rigorous analysis was used in this study. The formations of
328 pNO_3^- and ClNO_2 were calculated and integrated based on the measured S_a and N_2O_5 from 5 min-
329 averaged datasets and an estimated initial γ and f . The γ and f were optimized until good agreement
330 between the observed and predicted concentrations of pNO_3^- and ClNO_2 was obtained. Figure 6 depicts
331 an example of the fitting results on May 28, the predicted N_2O_5 uptake coefficient and ClNO_2 yield
332 were 0.017 and 1.0, respectively. Five sets of values of γ and f obtained are listed in Table 4. N_2O_5
333 uptake coefficients ranged from 0.012 - 0.055, with an average of 0.034 ± 0.018 , and the ClNO_2 yield
334 ranged from 0.50 to unity, with an average of 0.73 ± 0.25 . The errors from each derivation were 30%
335 - 50% and came from the field measurements of S_a , N_2O_5 , pNO_3^- and ClNO_2 .

336 The average γ value was consistent with the results derived by the same method in a rural site in
337 Germany (Phillips et al., 2016) but was higher than that found in previous studies in the UK and North
338 America that used different derivation methods; these methods included the steady state lifetime
339 method (Morgan et al., 2015; Brown et al., 2006, 2009), the iterated box model (Wagner et al., 2013)
340 and direct measurement based on an aerosol flow reactor (Bertram et al., 2009; Riedel et al., 2012).
341 The steady state lifetime method is very sensitive to NO_2 concentration, and since the NO_2
342 measurement suffered with ambient NO_y interference, we did not apply the steady state lifetime
343 method in this study (Brown et al., 2003). Nonetheless, the derived γ in Beijing showed good
344 agreement with the recent results derived by the steady state method in Jinan and Mt. Tai (X. F. Wang
345 et al., 2017; Z. Wang et al., 2017). The consistency eliminates the discrepancy possibly brought by
346 the differences of analysis methods. Therefore, we suggest that fast N_2O_5 uptake was a ubiquitous
347 feature that existed in the NCP. In this study, sulfate is dominated the $\text{PM}_{1.0}$ concentration with the
348 percentage over 30%, which may be the reason of elevated N_2O_5 uptake coefficient presented in
349 Beijing, like the result in high sulfate air mass over Ohio and western Pennsylvania (Brown et al.,
350 2006). Previous studies have shown that the N_2O_5 uptake coefficient strongly depends on the liquid
351 water, the pNO_3^- and organic mass; liquid water content promotes N_2O_5 uptake, whereas pNO_3^- and
352 organic mass inhibit N_2O_5 uptake (Thornton et al., 2003; Wahner et al., 1998; McNeill et al., 2006).
353 Because of the limited data set of N_2O_5 uptake coefficients in this campaign, the trends of the
354 determined N_2O_5 uptake coefficients with the parameters mentioned above were not convincing, and
355 more valid data is needed for further studies of the N_2O_5 uptake mechanism. With respect to f , the



356 values are comparable with that observed in Germany (Phillips et al., 2016) and are similar with that
357 estimated in the power plant plume in Mt. Tai with high chloride content (Z. Wang et al., 2017).

358 **4.2 N₂O₅ lifetime and reactivity**

359 The lifetime of N₂O₅ was estimated by the steady state method, assuming that the production and loss
360 of N₂O₅ was in balance after a period following sunset. Eq. 2 for the steady state approximation has
361 been frequently applied in analyzing the fate of N₂O₅ (Platt et al., 1980; Allan et al., 1999; Brown et
362 al., 2003).

363
$$\tau_{ss}(N_2O_5) = \frac{1}{L_{ss}(N_2O_5)} = \frac{[N_2O_5]}{k_{NO_2+O_3}[NO_2][O_3]} \quad (\text{Eq. 2})$$

364 In Eq. 2 $\tau_{ss}(N_2O_5)$ denotes the steady state lifetime of N₂O₅ and $L_{ss}(N_2O_5)$ denotes the loss term of
365 N₂O₅ corresponding to the steady state lifetime. A numerical model was used to check the validity of
366 the steady state approximation (Brown et al., 2003); details are given in Figure S2. The results show
367 that the steady state can generally be achieved within 30 minutes. In this study, the steady state lifetime
368 was only calculated from 20:00 to 04:00. The time periods with NO concentration larger than 0.1 ppbv
369 were excluded because the steady state is easily disturbed. The overall N₂O₅ reactivity ($k(N_2O_5)$) can
370 be calculated by accumulating each individual loss term as in Eq. 3, including the N₂O₅ heterogeneous
371 hydrolysis and the reaction of NO₃ with VOCs. The NO₃ heterogeneous uptake and the loss of N₂O₅
372 via gas-phase reactions were assumed to be negligible (Brown and Stutz, 2012). k_i represent the
373 reaction rate constants of the reaction of NO₃+VOC_i. Isoprene and monoterpane were used in the
374 calculation. The N₂O₅ loss rate coefficient by heterogeneous hydrolysis was calculated by using an
375 average γ of 0.034.

376
$$k(N_2O_5) = \frac{\sum k_i [VOCs_i]}{k_{eq} \cdot [NO_2]} + \frac{C \cdot S_a \gamma}{4} \quad (\text{Eq. 3})$$

377 The time series of the steady state lifetime of N₂O₅ is shown in Figure S3. The N₂O₅ steady state
378 lifetime ranged from <5 s to 1140 s, with an average of 310 ± 240 s, and large variability was shown
379 during the campaign. The N₂O₅ lifetimes during the BAM period were higher than those during the
380 UAM period, which is predictable since the clean air mass has lower N₂O₅ reactivity because of much
381 lower aerosol loading. Two extremely short N₂O₅ lifetime cases were captured on the nights of May
382 30 and June 3, with peak values below 200 s throughout those nights. Figure 7 shows that the N₂O₅
383 lifetime had a very clear negative dependence of the ambient aerosol surface area when larger than
384 $300 \mu\text{m}^2 \text{cm}^{-3}$, which indicates that the N₂O₅ heterogeneous uptake plays an important role in the
385 regulation of N₂O₅ lifetime. The study conducted in the residual layer of Hong Kong showed a similar
386 tendency despite the overall N₂O₅ lifetime being shorter at this site (Brown et al., 2016). Additionally,
387 a negative dependence of N₂O₅ lifetime on RH was reported in Hong Kong but was not observed in
388 this study (Figure S4).

389 Figure 8 shows the time series of the overall N₂O₅ loss rate constant as well as the steady state N₂O₅
390 loss rate. The overall N₂O₅ loss rate constant from the individuals was reasonably comparable with the
391 steady state N₂O₅ loss rate, except for the nights of 28, 30 May and 3 June, on which the $L_{ss}(N_2O_5)$



392 calculated by the steady state method were much higher than the overall $k(\text{N}_2\text{O}_5)$. The average N_2O_5
393 loss rate contributed by the N_2O_5 heterogeneous hydrolysis was $8.1 \times 10^{-4} \text{ s}^{-1}$. The average NO_3 loss rate
394 by the reaction of NO_3 with VOCs was $0.015 \pm 0.007 \text{ s}^{-1}$, which is comparable with the previous results
395 in suburban Beijing in 2006 (H. C. Wang et al., 2017c), in which the contribution to the N_2O_5 reactivity
396 was $1.63 \times 10^{-3} \text{ s}^{-1}$. Compared with N_2O_5 loss via direct heterogeneous hydrolysis, the indirect loss via
397 NO_3+VOCs as dominated by approximately 67% of the total N_2O_5 loss. Because only a subset of the
398 suite of organic species at the site was measured, the calculated loss rate constant via NO_3+VOCs
399 represents a lower limit. Therefore, the N_2O_5 loss via NO_3+VOCs may occupy a larger proportion. The
400 overall loss rate constant from NO_3+VOCs and N_2O_5 uptake was $2.44 \times 10^{-3} \text{ s}^{-1}$, which was reasonably
401 lower than the steady state N_2O_5 loss rate constant of $3.61 \times 10^{-3} \text{ s}^{-1}$; the gap may be explained by the
402 unmeasured reactive VOCs or the unaccounted NO that was near the instrumental limit of detection.

403 4.3 Nocturnal NO_3 oxidation

404 Recent studies have suggested that the fate of BVOCs after sunset is dominated by NO_x or O_3 , with
405 variation of the ratio of NO_x to BVOCs and that the nighttime oxidation is located in the transition
406 region between NO_x -domination and O_3 -domination in the United States (Edwards et al., 2017).
407 During this campaign, the nocturnal average concentrations of isoprene and monoterpene were $156 \pm$
408 88 pptv and 86 ± 42 pptv, respectively. We used isoprene and monoterpene to represent a lower limit
409 mixing ratio of total BVOCs; the average ratio of NO_x/BVOC was larger than 10 and exhibited small
410 variation during the BAM and UAM periods. The value was much higher than the critical value
411 ($\text{NO}_x/\text{BVOC} = 0.5$) of the transition regime proposed by Edwards et al. (2017), which suggests that
412 the oxidation of BVOCs in Beijing was NO_x -dominated and the nighttime fate of BVOCs was
413 controlled by NO_3 . Since the ONs formation via BVOC oxidation was mainly attributed to the NO_3
414 oxidation with high yield, we suggest that the ONs production capacity was maximized in the high
415 NO_x/BVOCs region.

416 Similar to $k(\text{OH})$, the nighttime VOCs reactivity, $k(\text{VOCs}_i)$, is defined as the pseudo loss rate of
417 VOCs oxidized by oxidants and is expressed as Eq. 4. Here, we only consider the oxidation by O_3 and
418 NO_3 . $k_{\text{VOCs}_i+\text{NO}_3}$ and $k_{\text{VOCs}_i+\text{O}_3}$ are the reaction constants of VOCs_i with NO_3 and O_3 , respectively.

$$419 \quad k(\text{VOCs}_i) = k_{\text{VOCs}_i+\text{NO}_3} \cdot [\text{NO}_3] + k_{\text{VOCs}_i+\text{O}_3} \cdot [\text{O}_3] \quad (\text{Eq. 4})$$

420 During this campaign, VOCs reactivity could be determined with the measured O_3 and calculated NO_3 .
421 Figure 9 depicts four kinds of VOCs reactivity distribution during nighttime, including the isoprene
422 (ISO), monoterpene (here represented by α -pinene, API), the alkenes with the double bond elsewhere
423 in the molecule (OLI) and the double bond at the end or terminal position of the molecule (OLT). The
424 reaction rates were cited from the regional atmospheric chemistry mechanism version 2 (RACM2,
425 Goliff et al., (2013)). The VOCs reactivity were dominated by NO_3 oxidation and contributed up to
426 90% in total; less than 10% were oxidized by O_3 during the nighttime. The results further confirmed
427 that the oxidation of BVOCs is controlled by NO_3 rather than O_3 .

428 For calculating nocturnal ONs production from NO_3 oxidation of isoprene and monoterpene, as well
429 as the same period inorganic nitrate production via N_2O_5 heterogeneous uptake, the ClNO_2 yield was



430 set to the determined average value of 0.73. The organic nitrate yield of the reaction of NO_3 with
431 isoprene was set to 0.7, from Rollins et al. (2009). The yield from the reaction of NO_3 with
432 monoterpene was represented by the $\text{NO}_3 + \alpha\text{-pinene}$ and was set to 0.15, following Spittler et al. (2006).
433 Although the yield from the NO_3 oxidation of isoprene is much higher than that of monoterpene, the
434 total ONs production was dominated by the oxidation of NO_3 with monoterpene because the reaction
435 of NO_3 with monoterpene is much faster than that with isoprene. Because of the lack of measurement
436 of alkenes and other VOCs that can react with NO_3 and form ONs, the calculated nighttime ONs
437 production rate analyzed here served as lower limit estimations. Figure 10 depicts the mean diurnal
438 profiles of the nocturnal formation rates of inorganic nitrates and ONs. The average production rate of
439 ONs was up to $0.11 \pm 0.09 \text{ ppbv h}^{-1}$, which was much higher than that predicted in a suburban site in
440 Beijing in 2006, with an average value of 0.06 ppbv h^{-1} (H. C. Wang et al., 2017b). In the high
441 NOx/BVOCs air masses, the inorganic nitrate formation was proposed to increase with the increase of
442 sunset NOx/BVOCs (Edwards et al., 2017). The formation rate of inorganic nitrate via N_2O_5 uptake
443 was significant, with an average of $0.43 \pm 0.12 \text{ ppbv h}^{-1}$, and was much larger than the organic nitrate
444 formation. The NOx was mainly removed as the inorganic nitrate format by nocturnal $\text{NO}_3\text{-N}_2\text{O}_5$
445 chemistry in Beijing. Overall, the $\text{NO}_3\text{-N}_2\text{O}_5$ chemistry promoted significant NOx removal, with 0.54
446 ppbv h^{-1} accounted for by the organic and inorganic nitrates, and the integral NOx removal was
447 approximately 5 ppbv per night. Since ONs is an important precursor of the secondary organic aerosols
448 (SOA), the NO_3 oxidation was very important from the perspective of organic aerosol formation and
449 regional particulate matter (e.g., Ng et al., 2008).

450

451 5. Conclusion

452 We reported an intensive field study of $\text{NO}_3\text{-N}_2\text{O}_5$ chemistry at a downwind suburban site in Beijing
453 during the summer of 2016. High levels of ClNO_2 and N_2O_5 were observed, with maxima of 2.9 ppbv
454 and 937 pptv (1-min), respectively. The N_2O_5 uptake coefficient was estimated to be in the range of
455 0.012-0.055, with an average value of 0.034 ± 0.018 , and the corresponding ClNO_2 yield was derived
456 to be in the range of 0.5-1.0, with an average value of 0.73 ± 0.25 . The elevated ClNO_2 levels and
457 $\text{ClNO}_2/\text{N}_2\text{O}_5$ ratios are comparable with those in chloride-rich regions in the NCP. The results highlight
458 fast N_2O_5 heterogeneous hydrolysis and efficient ClNO_2 formation in the outflow of urban Beijing.
459 Thus, its role in O_3 pollution in summer could be more important than in other regions.

460 Since the $\text{NO}_3\text{-N}_2\text{O}_5$ chemical equilibrium favors NO_3 in summer with high temperature and high
461 NOx, the elevated NO_3 dominated the nocturnal degradation of BVOCs and could lead to efficient
462 ONs formation. Because the air masses in Beijing featured high NOx/BVOCs ratios (>10), our results
463 suggest that the nocturnal NO_3 oxidation of BVOCs was NOx-dominated. Because of the extremely
464 high NOx emissions, the formation of ONs may not be sensitive to the reduction of NOx but rather to
465 the change of unsaturated VOCs (e.g., BVOCs), which is similar to the daytime photochemical O_3
466 pollution (e.g., Lu et al., 2010) diagnosed for this area; this suggests that the control of the unsaturated
467 VOCs would moderate the O_3 pollution and ONs particulate matter in parallel. Moreover, the reduction
468 of NOx would also be helpful to reduce the pNO_3^- formation via N_2O_5 heterogeneous hydrolysis under
469 such high NOx/BVOCs ratios (Edwards et al., 2017).



470 **Acknowledgements.** This work was supported by the National Natural Science Foundation of China
471 (Grants No. 91544225, 41375124, 21522701, 41421064, 91744204), the Strategic Priority Research
472 Program of the Chinese Academy of Sciences (Grants No. XDB05010500), the program on
473 ‘Photochemical smog in China’ financed by the Swedish Research Council (639-2013-6917), and the
474 National Key R&D Program of China (Grants No. 2016YFC0202000, Task 3). The authors gratefully
475 acknowledge the Peking University and Gethenborg University science team for their technical support
476 and discussions during the Changping campaign.

477

478 **Reference**

479

480 Allan, B. J., Carslaw, N., Coe, H., Burgess, R. A., and Plane, J. M. C.: Observations of the nitrate radical in the marine
481 boundary layer, *J Atmos Chem*, 33, 129-154, Doi10.1023/A:1005917203307, 1999.

482 Bannan, T. J., Booth, A. M., Bacak, A., Muller, J. B. A., Leather, K. E., Le Breton, M., Jones, B., Young, D., Coe, H.,
483 Allan, J., Visser, S., Slowik, J. G., Furger, M., Prevot, A. S. H., Lee, J., Dunmore, R. E., Hopkins, J. R., Hamilton,
484 J. F., Lewis, A. C., Whalley, L. K., Sharp, T., Stone, D., Heard, D. E., Fleming, Z. L., Leigh, R., Shallcross, D.
485 E., and Percival, C. J.: The first UK measurements of nitryl chloride using a chemical ionization mass
486 spectrometer in central London in the summer of 2012, and an investigation of the role of Cl atom oxidation, *J*
487 *Geophys Res-Atmos*, 120, 5638-5657, 10.1002/2014jd022629, 2015.

488 Benton, A. K., Langridge, J. M., Ball, S. M., Bloss, W. J., Dall'Osto, M., Nemitz, E., Harrison, R. M., and Jones, R.
489 L.: Night-time chemistry above London: measurements of NO_3 and N_2O_5 from the BT Tower, *Atmos Chem
490 Phys*, 10, 9781-9795, 10.5194/acp-10-9781-2010, 2010.

491 Bertram, T. H., and Thornton, J. A.: Toward a general parameterization of N_2O_5 reactivity on aqueous particles: the
492 competing effects of particle liquid water, nitrate and chloride, *Atmos Chem Phys*, 9, 8351-8363, 2009.

493 Bertram, T. H., Thornton, J. A., Riedel, T. P., Middlebrook, A. M., Bahreini, R., Bates, T. S., Quinn, P. K., and
494 Coffman, D. J.: Direct observations of N_2O_5 reactivity on ambient aerosol particles, *Geophys Res Lett*, 36, Artn
495 L19803.10.1029/2009gl040248, 2009.

496 Bohn, B., Corlett, G. K., Gillmann, M., Sanghavi, S., Stange, G., Tensing, E., Vrekoussis, M., Bloss, W. J., Clapp, L.
497 J., Kortner, M., Dorn, H.-P., Monks, P. S., Platt, U., Plass-Dülmer, C., Mihalopoulos, N., Heard, D. E.,
498 Clemithshaw, K. C., Meixner, F. X., Prevot, A. S. H., and Schmitt, R.: Photolysis frequency measurement
499 techniques: results of a comparison within the ACCENTproject, *Atmos. Chem. Phys.*, 8, 5373-5391,
500 doi:10.5194/acp-8-5373-2008, 2008.

501 Boyd, C. M., Nah, T., Xu, L., Berkemeier, T., and Ng, N. L.: Secondary Organic Aerosol (SOA) from Nitrate Radical
502 Oxidation of Monoterpenes: Effects of Temperature, Dilution, and Humidity on Aerosol Formation, Mixing,
503 and Evaporation, *Environ Sci Technol*, 51, 7831-7841, 2017.

504 Brown, S. S., Stark, H., and Ravishankara, A. R.: Applicability of the steady state approximation to the interpretation
505 of atmospheric observations of NO_3 and N_2O_5 , *J Geophys Res-Atmos*, 108, Artn 4539.Doi
506 10.1029/2003jd003407, 2003.



507 Brown, S. S., Ryerson, T. B., Wollny, A. G., Brock, C. A., Peltier, R., Sullivan, A. P., Weber, R. J., Dube, W. P., Trainer,
508 M., Meagher, J. F., Fehsenfeld, F. C., and Ravishankara, A. R.: Variability in nocturnal nitrogen oxide processing
509 and its role in regional air quality, *Science*, 311, 67-70, DOI 10.1126/science.1120120, 2006.

510 Brown, S. S., Dube, W. P., Fuchs, H., Ryerson, T. B., Wollny, A. G., Brock, C. A., Bahreini, R., Middlebrook, A. M.,
511 Neuman, J. A., Atlas, E., Roberts, J. M., Osthoff, H. D., Trainer, M., Fehsenfeld, F. C., and Ravishankara, A. R.:
512 Reactive uptake coefficients for N_2O_5 determined from aircraft measurements during the Second Texas Air
513 Quality Study: Comparison to current model parameterizations, *J Geophys Res-Atmos*, 114, Artn D00f10. Doi
514 10.1029/2008jd011679, 2009.

515 Brown, S. S., and Stutz, J.: Nighttime radical observations and chemistry, *Chem Soc Rev*, 41, 6405-6447, Doi
516 10.1039/C2cs35181a, 2012.

517 Brown, S. S., Dube, W. P., Tham, Y. J., Zha, Q. Z., Xue, L. K., Poon, S., Wang, Z., Blake, D. R., Tsui, W., Parrish, D.
518 D., and Wang, T.: Nighttime chemistry at a high altitude site above Hong Kong, *J Geophys Res-Atmos*, 121,
519 2457-2475, 10.1002/2015jd024566, 2016.

520 Chang, W. L., Bhave, P. V., Brown, S. S., Riemer, N., Stutz, J., and Dabdub, D.: Heterogeneous Atmospheric
521 Chemistry, Ambient Measurements, and Model Calculations of N_2O_5 : A Review, *Aerosol Sci Tech*, 45, 665-695,
522 2011.

523 DeCarlo, P. F., Kimmel, J., Trimborn, A., Northway, M., Jayne, J. T., Aiken, A., Gonin, M., Fuhrer, K., Horvath, T.,
524 Docherty, K., Worsnop, D. R., and Jimenez, J. L.: Field-deployable, high-resolution, time-of-flight Aerosol Mass
525 Spectrometer, *Anal. Chem.*, 78, 8281-8289, 2006.

526 de Gouw, J. and Warneke, C.: Measurements of volatile organic compounds in the earth's atmosphere using proton-
527 transferreaction mass spectrometry, *Mass Spectrom. Rev.*, 26, 223-257, 2007.

528 Dong, H. B., Zeng, L. M., Hu, M., Wu, Y. S., Zhang, Y. H., Slanina, J., Zheng, M., Wang, Z. F., and Jansen, R.:
529 Technical Note: The application of an improved gas and aerosol collector for ambient air pollutants in China,
530 *Atmos Chem Phys*, 12, 10519-10533, 2012.

531 Draxler, R. R., and G. D. Rolph: HYSPLIT (HYbrid Single-Particle Lagrangian Integrated Tracker) Model access
532 via NOAA ARL Ready Website [Available at <http://www.arl.noaa.gov/ready/hysplit4.html>, NOAA Air
533 Resources Laboratory, Silver Spring, MD]. 2003.

534 Edwards, P. M., Aikin, K. C., Dube, W. P., Fry, J. L., Gilman, J. B., de Gouw, J. A., Graus, M. G., Hanisco, T. F.,
535 Holloway, J., Huber, G., Kaiser, J., Keutsch, F. N., Lerner, B. M., Neuman, J. A., Parrish, D. D., Peischl, J.,
536 Pollack, I. B., Ravishankara, A. R., Roberts, J. M., Ryerson, T. B., Trainer, M., Veres, P. R., Wolfe, G. M.,
537 Warneke, C., and Brown, S. S.: Transition from high- to low- NO_x control of night-time oxidation in the
538 southeastern US, *Nat Geosci*, 10, 490-+, 10.1038/Ngeo2976, 2017.

539 Faxon, C. B., Bean, J. K., and Ruiz, L. H.: Inland Concentrations of Cl_2 and ClNO_2 in Southeast Texas suggest
540 chlorine chemistry significantly contributes to atmospheric reactivity, *Atmosphere*, 6, 1487-1506, 2015.

541 Finlaysonpitts, B. J., Ezell, M. J., and Pitts, J. N.: Formation of Chemically Active Chlorine Compounds by Reactions
542 of Atmospheric NaCl Particles with Gaseous N_2O_5 and ClONO_2 , *Nature*, 337, 241-244, DOI 10.1038/337241a0,
543 1989.



544 Fry, J. L., Kiendler-Scharr, A., Rollins, A. W., Wooldridge, P. J., Brown, S. S., Fuchs, H., Dube, W., Mensah, A., dal
545 Maso, M., Tillmann, R., Dorn, H. P., Brauers, T., and Cohen, R. C.: Organic nitrate and secondary organic
546 aerosol yield from NO_3 oxidation of beta-pinene evaluated using a gas-phase kinetics/aerosol partitioning model,
547 *Atmos Chem Phys*, 9, 1431-1449, 2009.

548 Gaston, C. J., Thornton, J. A., and Ng, N. L.: Reactive uptake of N_2O_5 to internally mixed inorganic and organic
549 particles: the role of organic carbon oxidation state and inferred organic phase separations, *Atmos Chem Phys*,
550 14, 5693-5707, 10.5194/acp-14-5693-2014, 2014.

551 Geyer, A., Aliche, B., Konrad, S., Schmitz, T., Stutz, J., and Platt, U.: Chemistry and oxidation capacity of the nitrate
552 radical in the continental boundary layer near Berlin, *J Geophys Res-Atmos*, 106, 8013-8025, Doi
553 10.1029/2000jd900681, 2001.

554 Goliff, W. S., Stockwell, W. R., and Lawson, C. V.: The regional atmospheric chemistry mechanism, version 2, *Atmos*
555 *Environ*, 68, 174-185, 2013.

556 Grzinic, G., Bartels-Rausch, T., Berkemeier, T., Turler, A., and Ammann, M.: Viscosity controls humidity dependence
557 of N_2O_5 uptake to citric acid aerosol, *Atmos Chem Phys*, 15, 13615-13625, 2015.

558 Hallquist, M., Stewart, D. J., Stephenson, S. K., and Cox, R. A.: Hydrolysis of N_2O_5 on sub-micron sulfate aerosols,
559 *Phys Chem Chem Phys*, 5, 3453-3463, Doi 10.1039/B301827j, 2003.

560 Hallquist, M., Munthe, J., Hu, M., Wang, T., Chan, C. K., Gao, J., Boman, J., Guo, S., Hallquist, A. M., Mellqvist, J.,
561 Moldanova, J., Pathak, R. K., Pettersson, J. B. C., Pleijel, H., Simpson, D., and Thynell, M.: Photochemical
562 smog in China: scientific challenges and implications for air-quality policies, *Natl Sci Rev*, 3, 401-403,
563 10.1093/nsr/nww080, 2016.

564 Kiendler-Scharr, A., Mensah, A. A., Friese, E., Topping, D., Nemitz, E., Prevot, A. S. H., Aijala, M., Allan, J.,
565 Canonaco, F., Canagaratna, M., Carbone, S., Crippa, M., Dall Osto, M., Day, D. A., De Carlo, P., Di Marco, C.,
566 Elbern, H., Eriksson, A., Freney, E., Hao, L., Herrmann, H., Hildebrandt, L., Hillamo, R., Jimenez, J. L.,
567 Laaksonen, A., McFiggans, G., Mohr, C., O'Dowd, C., Otjes, R., Ovadnevaite, J., Pandis, S. N., Poulain, L.,
568 Schlag, P., Sellegrí, K., Swietlicki, E., Tiiitta, P., Vermeulen, A., Wahner, A., Worsnop, D., and Wu, H. C.:
569 Ubiquity of organic nitrates from nighttime chemistry in the European submicron aerosol, *Geophys Res Lett*,
570 43, 7735-7744, 2016.

571 Le Breton, M., Bacak, A., Muller, J. B. A., Bannan, T. J., Kennedy, O., Ouyang, B., Xiao, P., Bauguitte, S. J. B.,
572 Shallcross, D. E., Jones, R. L., Daniels, M. J. S., Ball, S. M., and Percival, C. J.: The first airborne comparison
573 of N_2O_5 measurements over the UK using a CIMS and BBCEAS during the RONOCO campaign, *Anal*
574 *Methods-Uk*, 6, 9731-9743, 10.1039/c4ay02273d, 2014.

575 Le Breton, M., Hallquist, Å. M., Pathak, R. K., Simpson, D., Wang, Y., Johansson, J., Zheng, J., Yang, Y., Shang, D.,
576 Wang, H., Liu, Q., Chan, C., Wang, T., Bannan, T. J., Priestley, M., Percival, C. J., Shallcross, D. E., Lu, K.,
577 Guo, S., Hu, M., and Hallquist, M.: Chlorine oxidation of VOCs at a semi-rural site in Beijing: Significant
578 chlorine liberation from ClNO_2 and subsequent gas and particle phase Cl-VOC production, *Atmos. Chem. Phys.*
579 *Discuss.*, 2018, 1-25, 2018.



580 Li, S. W., Liu, W. Q., Xie, P. H., Qin, M., and Yang, Y. J.: Observation of Nitrate Radical in the Nocturnal Boundary
581 Layer During a Summer Field Campaign in Pearl River Delta, China, *Terr Atmos Ocean Sci*, 23, 39-48, Doi
582 10.3319/Tao.2011.07.26.01(a), 2012.

583 Li, Q. Y., Zhang, L., Wang, T., Tham, Y. J., Ahmadov, R., Xue, L. K., Zhang, Q., and Zheng, J. Y.: Impacts of
584 heterogeneous uptake of dinitrogen pentoxide and chlorine activation on ozone and reactive nitrogen
585 partitioning: improvement and application of the WRF-Chem model in southern China, *Atmos Chem Phys*, 16,
586 14875-14890, 10.5194/acp-16-14875-2016, 2016.

587 Liu, X. G., Gu, J. W., Li, Y. P., Cheng, Y. F., Qu, Y., Han, T. T., Wang, J. L., Tian, H. Z., Chen, J., and Zhang, Y. H.:
588 Increase of aerosol scattering by hygroscopic growth: Observation, modeling, and implications on visibility,
589 *Atmos Res*, 132, 91-101, 10.1016/j.atmosres.2013.04.007, 2013.

590 Liu, M. X., Song, Y., Zhou, T., Xu, Z. Y., Yan, C. Q., Zheng, M., Wu, Z. J., Hu, M., Wu, Y. S., and Zhu, T.: Fine
591 particle pH during severe haze episodes in northern China, *Geophys Res Lett*, 44, 5213-5221,
592 10.1002/2017gl073210, 2017.

593 Lopez-Hilfiker, F. D., Mohr, C., Ehn, M., Rubach, F., Kleist, E., Wildt, J., Mentel, T. F., Lutz, A., Hallquist, M.,
594 Worsnop, D., and Thornton, J. A.: A novel method for online analysis of gas and particle composition:
595 description and evaluation of a Filter Inlet for Gases and AERosols (FIGAERO), *Atmos Meas Tech*, 7, 983-
596 1001, 10.5194/amt-7-983-2014, 2014.

597 Lu, K. D., Zhang, Y. H., Su, H., Brauers, T., Chou, C. C., Hofzumahaus, A., Liu, S. C., Kita, K., Kondo, Y., Shao, M.,
598 Wahner, A., Wang, J. L., Wang, X. S., and Zhu, T.: Oxidant ($O_3 + NO_2$) production processes and formation
599 regimes in Beijing, *J Geophys Res-Atmos*, 115, 2010.

600 McLaren, R., Wojtal, P., Majonis, D., McCourt, J., Halla, J. D., and Brook, J.: NO_3 radical measurements in a polluted
601 marine environment: links to ozone formation, *Atmos Chem Phys*, 10, 4187-4206, 10.5194/acp-10-4187-2010,
602 2010.

603 McNeill, V. F., Patterson, J., Wolfe, G. M., and Thornton, J. A.: The effect of varying levels of surfactant on the
604 reactive uptake of N_2O_5 to aqueous aerosol, *Atmos Chem Phys*, 6, 1635-1644, 2006.

605 Mentel, T. F., Sohn, M., and Wahner, A.: Nitrate effect in the heterogeneous hydrolysis of dinitrogen pentoxide on
606 aqueous aerosols, *Phys Chem Chem Phys*, 1, 5451-5457, Doi 10.1039/A905338g, 1999.

607 Mielke, L. H., Stutz, J., Tsai, C., Hurlock, S. C., Roberts, J. M., Veres, P. R., Froyd, K. D., Hayes, P. L., Cubison, M.
608 J., Jimenez, J. L., Washenfelder, R. A., Young, C. J., Gilman, J. B., de Gouw, J. A., Flynn, J. H., Grossberg, N.,
609 Lefer, B. L., Liu, J., Weber, R. J., and Osthoff, H. D.: Heterogeneous formation of nitryl chloride and its role as
610 a nocturnal NOx reservoir species during CalNex-LA 2010, *J Geophys Res-Atmos*, 118, 10638-10652, Doi
611 10.1002/Jgrd.50783, 2013.

612 Morgan, W. T., Ouyang, B., Allan, J. D., Aruffo, E., Di Carlo, P., Kennedy, O. J., Lowe, D., Flynn, M. J., Rosenberg,
613 P. D., Williams, P. I., Jones, R., McFiggans, G. B., and Coe, H.: Influence of aerosol chemical composition on
614 N_2O_5 uptake: airborne regional measurements in northwestern Europe, *Atmos Chem Phys*, 15, 973-990, DOI
615 10.5194/acp-15-973-2015, 2015.



616 Ng, N. L., Kwan, A. J., Surratt, J. D., Chan, A. W. H., Chhabra, P. S., Sorooshian, A., Pye, H. O. T., Crounse, J. D.,
617 Wennberg, P. O., Flagan, R. C., and Seinfeld, J. H.: Secondary organic aerosol (SOA) formation from reaction
618 of isoprene with nitrate radicals (NO₃), *Atmos Chem Phys*, 8, 4117-4140, 2008.

619 Ng, N. L., Brown, S. S., Archibald, A. T., Atlas, E., Cohen, R. C., Crowley, J. N., Day, D. A., Donahue, N. M., Fry,
620 J. L., Fuchs, H., Griffin, R. J., Guzman, M. I., Herrmann, H., Hodzic, A., Inuma, Y., Jimenez, J. L., Kiendler-
621 Scharr, A., Lee, B. H., Luecken, D. J., Mao, J. Q., McLaren, R., Mutzel, A., Osthoff, H. D., Ouyang, B., Picquet-
622 Varrault, B., Platt, U., Pye, H. O. T., Rudich, Y., Schwantes, R. H., Shiraiwa, M., Stutz, J., Thornton, J. A.,
623 Tilgner, A., Williams, B. J., and Zaveri, R. A.: Nitrate radicals and biogenic volatile organic compounds:
624 oxidation, mechanisms, and organic aerosol, *Atmos Chem Phys*, 17, 2103-2162, 10.5194/acp-17-2103-2017,
625 2017.

626 Osthoff, H. D., Roberts, J. M., Ravishankara, A. R., Williams, E. J., Lerner, B. M., Sommariva, R., Bates, T. S.,
627 Coffman, D., Quinn, P. K., Dibb, J. E., Stark, H., Burkholder, J. B., Talukdar, R. K., Meagher, J., Fehsenfeld, F.
628 C., and Brown, S. S.: High levels of nitryl chloride in the polluted subtropical marine boundary layer, *Nat Geosci*,
629 1, 324-328, Doi 10.1038/Ngeo177, 2008.

630 Phillips, G. J., Thieser, J., Tang, M. J., Sobanski, N., Schuster, G., Fachinger, J., Drewnick, F., Borrmann, S.,
631 Bingemer, H., Lelieveld, J., and Crowley, J. N.: Estimating N₂O₅ uptake coefficients using ambient
632 measurements of NO₃, N₂O₅, ClNO₂ and particle-phase nitrate, *Atmos Chem Phys*, 16, 13231-13249,
633 10.5194/acp-16-13231-2016, 2016.

634 Platt, U., Perner, D., Winer, A. M., Harris, G. W., and Pitts, J. N.: Detection of NO₃ in the Polluted Troposphere by
635 Differential Optical-Absorption, *Geophys Res Lett*, 7, 89-92, Doi 10.1029/GI007i001p00089, 1980.

636 Pye, H. O. T., Chan, A. W. H., Barkley, M. P., and Seinfeld, J. H.: Global modeling of organic aerosol: the importance
637 of reactive nitrogen (NO_x and NO₃), *Atmos Chem Phys*, 10, 11261-11276, 2010.

638 Riedel, T. P., Bertram, T. H., Ryder, O. S., Liu, S., Day, D. A., Russell, L. M., Gaston, C. J., Prather, K. A., and
639 Thornton, J. A.: Direct N2O5 reactivity measurements at a polluted coastal site, *Atmos Chem Phys*, 12, 2959-
640 2968, DOI 10.5194/acp-12-2959-2012, 2012.

641 Riedel, T. P., Wolfe, G. M., Danas, K. T., Gilman, J. B., Kuster, W. C., Bon, D. M., Vlasenko, A., Li, S. M., Williams,
642 E. J., Lerner, B. M., Veres, P. R., Roberts, J. M., Holloway, J. S., Lefer, B., Brown, S. S., and Thornton, J. A.:
643 An MCM modeling study of nitryl chloride (ClNO₂) impacts on oxidation, ozone production and nitrogen oxide
644 partitioning in polluted continental outflow, *Atmos Chem Phys*, 14, 3789-3800, 10.5194/acp-14-3789-2014,
645 2014.

646 Riemer, N., Vogel, H., Vogel, B., Anttila, T., Kiendler-Scharr, A., and Mentel, T. F.: Relative importance of organic
647 coatings for the heterogeneous hydrolysis of N₂O₅ during summer in Europe, *J Geophys Res-Atmos*, 114, 2009.

648 Roberts, J. M., Osthoff, H. D., Brown, S. S., Ravishankara, A. R., Coffman, D., Quinn, P., and Bates, T.: Laboratory
649 studies of products of N₂O₅ uptake on Cl⁻ containing substrates, *Geophys Res Lett*, 36, Artn L20808.
650 10.1029/2009gl040448, 2009.



651 Rollins, A. W., Kiendler-Scharr, A., Fry, J. L., Brauers, T., Brown, S. S., Dorn, H. P., Dube, W. P., Fuchs, H., Mensah,
652 A., Mentel, T. F., Rohrer, F., Tillmann, R., Wegener, R., Wooldridge, P. J., and Cohen, R. C.: Isoprene oxidation
653 by nitrate radical: alkyl nitrate and secondary organic aerosol yields, *Atmos Chem Phys*, 9, 6685-6703, 2009.

654 Sarwar, G., Simon, H., Xing, J., and Mathur, R.: Importance of tropospheric ClNO_2 chemistry across the Northern
655 Hemisphere, *Geophys Res Lett*, 41, 4050-4058, 10.1002/2014gl059962, 2014.

656 Spittler, M., Barnes, I., Bejan, I., Brockmann, K. J., Benter, T., and Wirtz, K.: Reactions of NO_3 radicals with limonene
657 and alpha-pinene: Product and SOA formation, *Atmos Environ*, 40, S116-S127,
658 10.1016/j.atmosenv.2005.09.093, 2006.

659 Stutz, J., Wong, K. W., Lawrence, L., Ziembka, L., Flynn, J. H., Rappengluck, B., and Lefer, B.: Nocturnal NO_3 radical
660 chemistry in Houston, TX, *Atmos Environ*, 44, 4099-4106, 10.1016/j.atmosenv.2009.03.004, 2010.

661 Su, X., Tie, X. X., Li, G. H., Cao, J. J., Huang, R. J., Feng, T., Long, X., and Xu, R. G.: Effect of hydrolysis of N_2O_5
662 on nitrate and ammonium formation in Beijing China: WRF-Chem model simulation, *Sci Total Environ*, 579,
663 221-229, 10.1016/j.scitotenv.2016.11.125, 2017.

664 Tan, Z., Fuchs, H., Lu, K., Hofzumahaus, A., Bohn, B., Broch, S., Dong, H., Gomm, S., Häseler, R., He, L., Holland,
665 F., Li, X., Liu, Y., Lu, S., Rohrer, F., Shao, M., Wang, B., Wang, M., Wu, Y., Zeng, L., Zhang, Y., Wahner, A.,
666 and Zhang, Y.: Radical chemistry at a rural site (Wangdu) in the North China Plain: observation and model
667 calculations of OH, HO_2 and RO_2 radicals, *Atmos. Chem. Phys.*, 17, 663-690, 10.5194/acp-17-663-2017, 2017.

668 Tang, M. J., Schuster, G., and Crowley, J. N.: Heterogeneous reaction of N_2O_5 with illite and Arizona test dust
669 particles, *Atmos Chem Phys*, 14, 245-254, 2014.

670 Tang, M. J., Thieser, J., Schuster, G., and Crowley, J. N.: Kinetics and mechanism of the heterogeneous reaction of
671 N_2O_5 with mineral dust particles, *Phys Chem Chem Phys*, 14, 8551-8561, 2012.

672 Tang, M., Huang, X., Lu, K., Ge, M., Li, Y., Cheng, P., Zhu, T., Ding, A., Zhang, Y., Gligorovski, S., Song, W., Ding,
673 X., Bi, X., and Wang, X.: Heterogeneous reactions of mineral dust aerosol: implications for tropospheric
674 oxidation capacity, *Atmos. Chem. Phys.*, 17, 11727-11777, <https://doi.org/10.5194/acp-17-11727-2017>, 2017.

675 Tham, Y. J., Wang, Z., Li, Q. Y., Yun, H., Wang, W. H., Wang, X. F., Xue, L. K., Lu, K. D., Ma, N., Bohn, B., Li, X.,
676 Kecorius, S., Gross, J., Shao, M., Wiedensohler, A., Zhang, Y. H., and Wang, T.: Significant concentrations of
677 nitril chloride sustained in the morning: investigations of the causes and impacts on ozone production in a
678 polluted region of northern China, *Atmos Chem Phys*, 16, 14959-14977, 10.5194/acp-16-14959-2016, 2016.

679 Thornton, J. A., Braban, C. F., and Abbatt, J. P. D.: N_2O_5 hydrolysis on sub-micron organic aerosols: the effect of
680 relative humidity, particle phase, and particle size, *Phys Chem Chem Phys*, 5, 4593-4603, Doi
681 10.1039/B307498f, 2003.

682 Thornton, J. A., and Abbatt, J. P. D.: N_2O_5 reaction on submicron sea salt aerosol: Kinetics, products, and the effect
683 of surface active organics, *J Phys Chem A*, 109, 10004-10012, Doi 10.1021/Jp054183t, 2005.

684 Thornton, J. A., Kercher, J. P., Riedel, T. P., Wagner, N. L., Cozic, J., Holloway, J. S., Dube, W. P., Wolfe, G. M.,
685 Quinn, P. K., Middlebrook, A. M., Alexander, B., and Brown, S. S.: A large atomic chlorine source inferred from
686 mid-continental reactive nitrogen chemistry, *Nature*, 464, 271-274, Doi 10.1038/Nature08905, 2010.



687 Wagner, N. L., Riedel, T. P., Young, C. J., Bahreini, R., Brock, C. A., Dube, W. P., Kim, S., Middlebrook, A. M.,
688 Ozturk, F., Roberts, J. M., Russo, R., Sive, B., Swarthout, R., Thornton, J. A., VandenBoer, T. C., Zhou, Y., and
689 Brown, S. S.: N₂O₅ uptake coefficients and nocturnal NO₂ removal rates determined from ambient wintertime
690 measurements, *J Geophys Res-Atmos*, 118, 9331-9350, Doi 10.1002/Jgrd.50653, 2013.

691 Wahner, A., Mentel, T. F., and Sohn, M.: Gas-phase reaction of N₂O₅ with water vapor: Importance of heterogeneous
692 hydrolysis of N₂O₅ and surface desorption of HNO₃ in a large teflon chamber, *Geophys Res Lett*, 25, 2169-
693 2172, Doi 10.1029/98gl51596, 1998.

694 Wang, S. S., Shi, C. Z., Zhou, B., Zhao, H., Wang, Z. R., Yang, S. N., and Chen, L. M.: Observation of NO₃ radicals
695 over Shanghai, China, *Atmos Environ*, 70, 401-409, DOI 10.1016/j.atmosenv.2013.01.022, 2013.

696 Wang, M., Shao, M., Chen, W., Yuan, B., Lu, S., Zhang, Q., Zeng, L., and Wang, Q.: A temporally and spatially
697 resolved validation of emission inventories by measurements of ambient volatile organic compounds in Beijing,
698 China, *Atmos Chem Phys*, 14, 5871-5891, 10.5194/acp-14-5871-2014, 2014.

699 Wang, D., Hu, R. Z., Xie, P. H., Liu, J. G., Liu, W. Q., Qin, M., Ling, L. Y., Zeng, Y., Chen, H., Xing, X. B., Zhu, G.
700 L., Wu, J., Duan, J., Lu, X., and Shen, L. L.: Diode laser cavity ring-down spectroscopy for in situ measurement
701 of NO₃ radical in ambient air, *J Quant Spectrosc Ra*, 166, 23-29, 10.1016/j.jqsrt.2015.07.005, 2015.

702 Wang, H. C., and Lu, K. D.: Determination and Parameterization of the Heterogeneous Uptake Coefficient of
703 Dinitrogen Pentoxide (N₂O₅), *Prog Chem*, 28, 917-933, 10.7536/Pc151225, 2016.

704 Wang, T., Tham, Y. J., Xue, L. K., Li, Q. Y., Zha, Q. Z., Wang, Z., Poon, S. C. N., Dube, W. P., Blake, D. R., Louie,
705 P. K. K., Luk, C. W. Y., Tsui, W., and Brown, S. S.: Observations of nitryl chloride and modeling its source and
706 effect on ozone in the planetary boundary layer of southern China, *J Geophys Res-Atmos*, 121, 2476-2489,
707 10.1002/2015jd024556, 2016.

708 Wang, H. C., Chen, J., and Lu, K. D.: Development of a portable cavity-enhanced absorption spectrometer for the
709 measurement of ambient NO₃ and N₂O₅: experimental setup, lab characterizations, and field applications in a
710 polluted urban environment, *Atmos Meas Tech*, 10, 1465-1479, 10.5194/amt-10-1465-2017, 2017a.

711 Wang, H. C., Lu, K. D., Tan, Z. F., Sun, K., Li, X., Hu, M., Shao, M., Zeng, L. M., Zhu, T., and Zhang, Y. H.:
712 Model simulation of NO₃, N₂O₅ and ClNO₂ at a rural site in Beijing during CAREBeijing-2006, *Atmos Res*,
713 196, 97-107, 10.1016/j.atmosres.2017.06.013, 2017b.

714 Wang, H. C., Lu, K. D., Chen, X. R., Zhu, Q. D., Chen, Q., Guo, S., Jiang, M. Q., Li, X., Shang, D. J., Tan, Z. F:
715 High N₂O₅ concentrations observed in urban Beijing: Implications of a large nitrate formation pathway, *Environ.
716 Sci. Technol. Lett.*, 10, doi: 10.1021/acs.estlett.7b00341, 2017c.

717 Wang, X. F., Wang, H., Xue, L. K., Wang, T., Wang, L. W., Gu, R. R., Wang, W. H., Tham, Y. J., Wang, Z., Yang, L.
718 X., Chen, J. M., and Wang, W. X.: Observations of N₂O₅ and ClNO₂ at a polluted urban surface site in North
719 China: High N₂O₅ uptake coefficients and low ClNO₂ product yields, *Atmos Environ*, 156, 125-134,
720 10.1016/j.atmosenv.2017.02.035, 2017.

721 Wang, Z., Wang, W. H., Tham, Y. J., Li, Q. Y., Wang, H., Wen, L., Wang, X. F., and Wang, T.: Fast heterogeneous
722 N₂O₅ uptake and ClNO₂ production in power plant and industrial plumes observed in the nocturnal residual
723 layer over the North China Plain, *Atmos Chem Phys*, 17, 12361-12378, 2017. 10.5194/acp-17-12361-2017



724 Wayne, R. P., Barnes, I., Biggs, P., Burrows, J. P., Canosamas, C. E., Hjorth, J., Lebras, G., Moortgat, G. K., Perner,
725 D., Poulet, G., Restelli, G., and Sidebottom, H.: The Nitrate Radical - Physics, Chemistry, and the Atmosphere,
726 Atmos Environ a-Gen, 25, 1-203, Doi 10.1016/0960-1686(91)90192-A, 1991.
727 Xue, L. K., Saunders, S. M., Wang, T., Gao, R., Wang, X. F., Zhang, Q. Z., and Wang, W. X.: Development of a
728 chlorine chemistry module for the Master Chemical Mechanism, Geosci Model Dev, 8, 3151-3162,
729 10.5194/gmd-8-3151-2015, 2015.
730 Ye, N. N. L., K. D. Dong, H. B. Wu, Y. S. Zeng, L. M and Zhang, Y. H.: A study of the Water-Soluble Inorganic Salts
731 and Their Gases Precursors at Wangdu Site in the Summer Time, Acta Scientiarum Naturalium Universitatis,
732 52, p1109-1117, doi.org/10.13209/j.0479-8023.2016.116, 2016.
733 Yue, D. L., Hu, M., Wu, Z. J., Wang, Z. B., Guo, S., Wehner, B., Nowak, A., Achtert, P., Wiedensohler, A., Jung, J.,
734 Kim, Y. J., and Liu, S.: Characteristics of aerosol size distributions and new particle formation in the summer in
735 Beijing, J Geophys Res-Atmos, 114, Artn D00g1210.1029/2008jd010894, 2009.
736 Zheng, J., Hu, M., Du, Z. F., Shang, D. J., Gong, Z. H., Qin, Y. H., Fang, J. Y., Gu, F. T., Li, M. R., Peng, J. F., Li, J.,
737 Zhang, Y. Q., Huang, X. F., He, L. Y., Wu, Y. S., and Guo, S.: Influence of biomass burning from South Asia at
738 a high-altitude mountain receptor site in China, Atmos Chem Phys, 17, 6853-6864, 10.5194/acp-17-6853-2017,
739 2017.
740

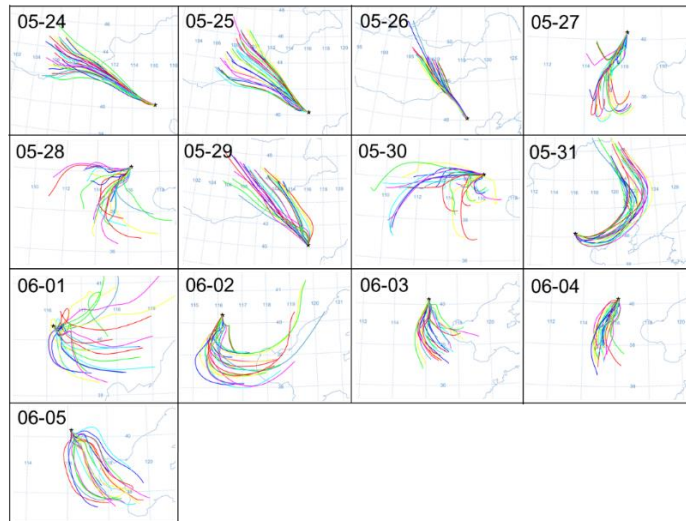


741



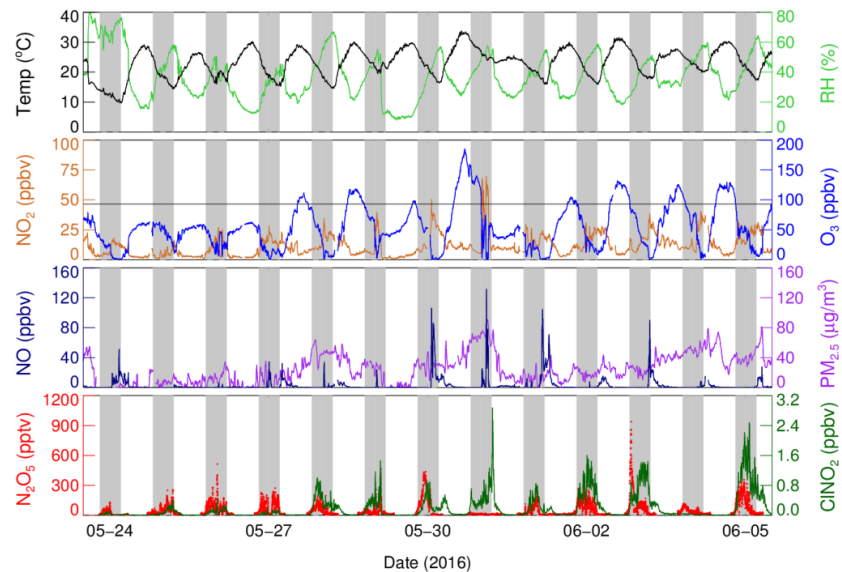
742 **Figure 1.** Map of Beijing and surrounding area. The red star represents the location of the Changping
743 sites, red dots show other sites where previous N_2O_5 measurements were conducted in the North China
744 Plain (NCP), including Peking University (PKU), Wangdu, Jinan and Mt. Tai (in Tai' an).

745



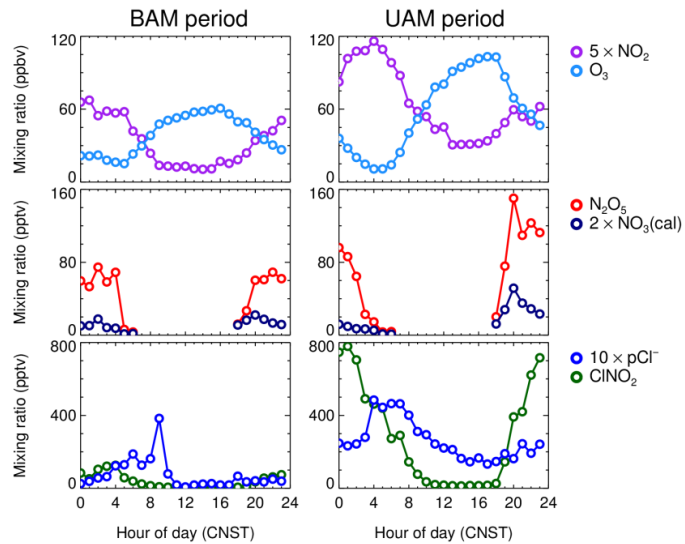
746

747 **Figure 2.** Backward trajectory calculations using the Hybrid Single-Particle Lagrangian Integrated
748 Trajectory (HYSPLIT) model. The images depict a 24-h history of air masses arriving at the
749 measurement site at 12:00 (CNST).



750

751 **Figure 3.** Time series of N_2O_5 , ClNO_2 and other relevant parameters. The black line in the O_3 panel
752 denotes Chinese national air quality standard for O_3 (ca. 93 ppbv for the surface conditions).



753

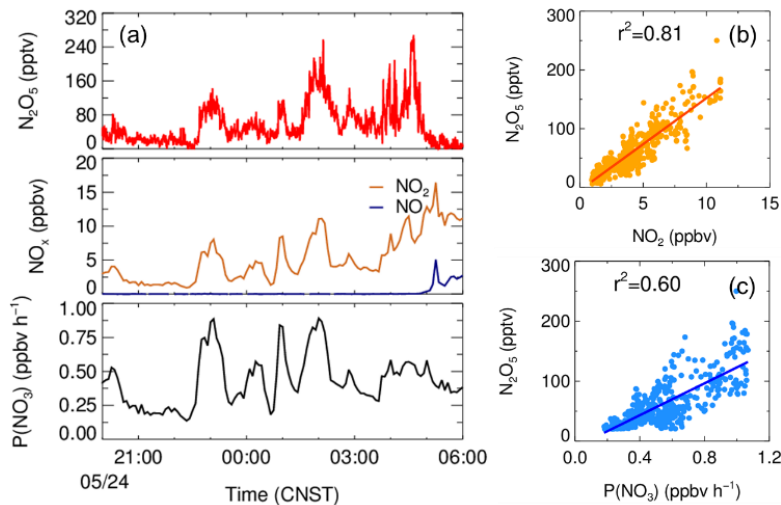
754 **Figure 4.** Mean diurnal profiles of $5 \times \text{NO}_2$, O_3 , N_2O_5 , $2 \times \text{NO}_3$ (calculated), ClNO_2 , and $10 \times \text{pCl}^-$. The
755 left three panels depict the background air mass (BAM) period and the right three panels depict the
756 urban air mass (UAM) period.



757

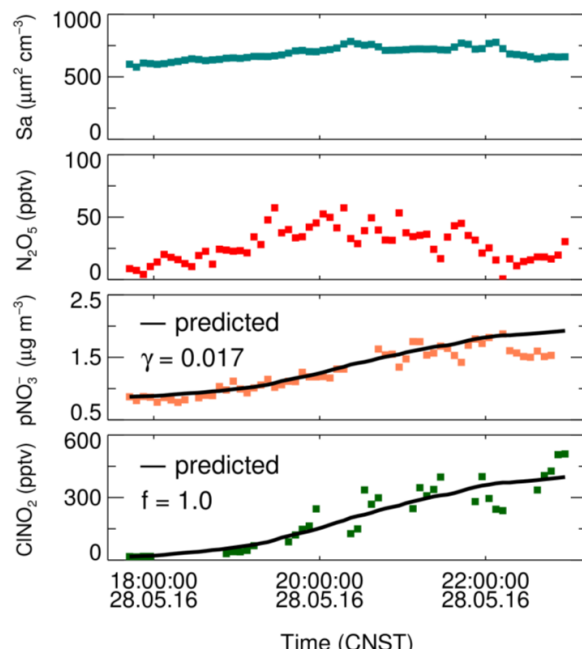
758 **Figure 5.** The correlation of the mixing ratio of N_2O_5 and NO_2 and the production rate of NO_3 on the
 759 night of May 24.

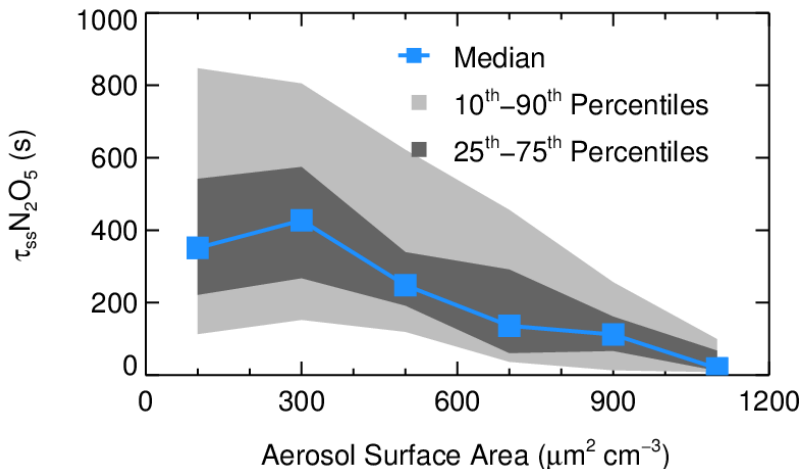
760



761

762 **Figure 6.** The best fitting of γ and f to reproduce the observed ClNO_2 and pNO_3^- with an offset on May
 763 28. The black lines are the predicted results of the integrated pNO_3^- and ClNO_2 by using the observed
 764 S_a and N_2O_5 .

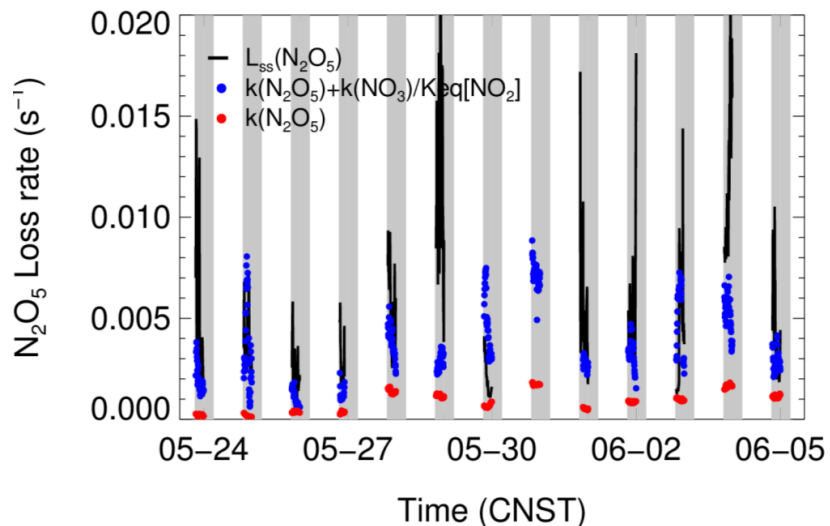




765

766 **Figure 7.** The dependence of N₂O₅ lifetime on aerosol surface area. Data were selected from 20:00 to
767 04:00 and are shown as medians, 25 - 75th percentile ranges, and 10 - 90th percentile ranges, as shown
768 in the legend.

769

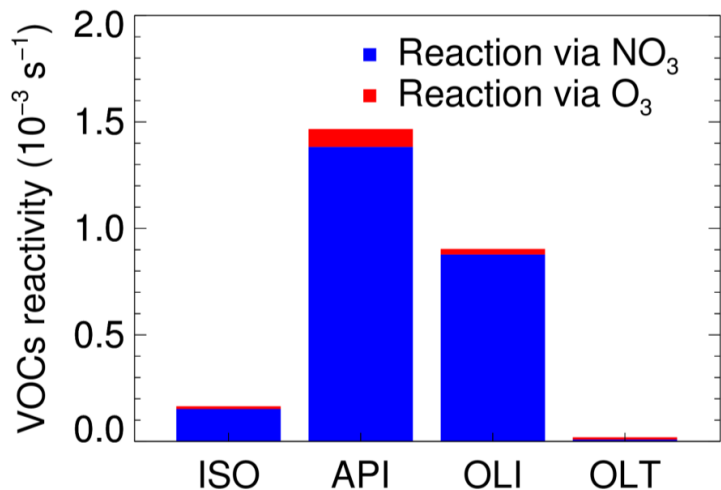


770

771 **Figure 8.** Time series of the individual N₂O₅ loss terms and the loss rate constant of N₂O₅ in steady
772 state ($L_{ss}(N_2O_5)$).

773

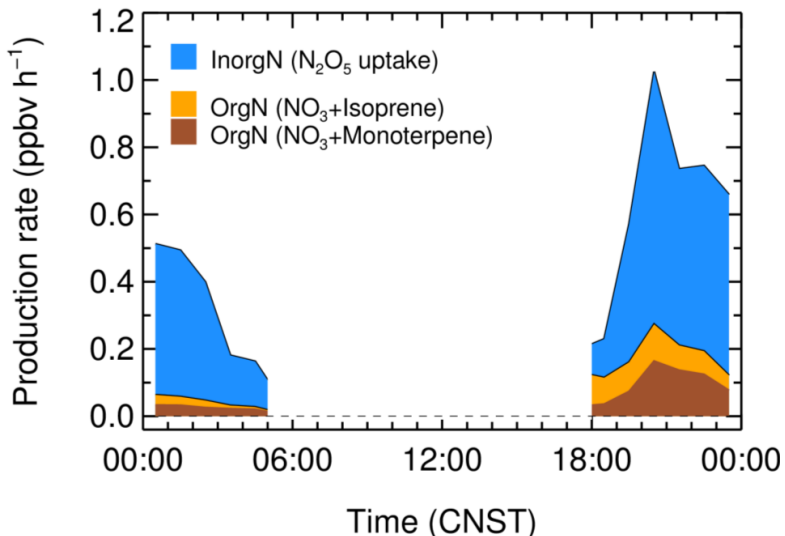
774



775

776 **Figure 9.** The nighttime VOCs reactivity of NO_3 and O_3 ; the classification was based on RACM2, and
777 data were selected from 20:00 to 04:00.

778



779

780 **Figure 10.** The nighttime production rate of organic and inorganic nitrates; the inorganic nitrates were
781 calculated from the N_2O_5 heterogeneous hydrolysis, and the ONs were calculated by the NO_3 reacted
782 with isoprene and monoterpene.

783



784

Table 1. The observed gas and particle parameters used in this analysis during the campaign.

| Species | Limit of detection | Methods | Accuracy |
|-------------------------------|--------------------------------------|------------------|-----------|
| N ₂ O ₅ | 2.7 pptv (1 σ , 1 min) | CEAS | \pm 19% |
| CINO ₂ | 16 pptv (2 σ , 1 min) | FIGAERO-ToF-CIMS | \pm 23% |
| NO | 60 pptv (2 σ , 1 min) | Mo convert | \pm 20% |
| NO ₂ | 0.3 ppbv (2 σ , 1 min) | Mo convert | \pm 20% |
| O ₃ | 0.5 ppbv (2 σ , 1 min) | UV photometry | \pm 5% |
| Aerosol surface area | - (4 min) | SMPS, APS | \pm 30% |
| VOCs | 0.1 ppbv (5 min) | PTR-MS | \pm 30% |
| PM _{2.5} | 0.1 μ g m ⁻³ (1 min) | TEOM | \pm 5% |
| PM _{1.0} components | 0.15 μ g m ⁻³ (4 min) | HR-ToF-AMS | \pm 30% |

785

786

Table 2. Summary of the field observed ambient CINO₂/N₂O₅

| Location | Region | CINO ₂ /N ₂ O ₅ ^a | References |
|--------------------|--------|---------------------------------------------------------------|-------------------------|
| Beijing, China | Inland | 0.7 – 42.0 (7.7) | This work |
| Wangdu, China | Inland | 0.4 - 131.3 (29.5) | Tham et al., 2016 |
| Jinan, China | Marine | 25.0 - 118.0 ^b | Z. Wang et al., 2017 |
| Mt. Tai, China | Marine | ~ 4.0 | X. F. Wang et al., 2017 |
| Hong Kong, China | Marine | 0.1 - 2.0 | T. Wang et al., 2016 |
| London, UK | Inland | 0.02 - 2.4 (0.51) | Bannan et al., 2015 |
| Frankfurt, Germany | Inland | 0.2 - 3.0 | Phillips et al., 2012 |
| Colorado, USA | Inland | 0.2 - 3.0 | Thornton et al., 2010 |
| California, USA | Marine | ~ 0.2 - 10.0 ^c | Mielke et al., 2013 |

787 Note: ^a Daily average results; ^b Power plant plume cases at Mt. Tai in Shandong, China; ^c Estimated according to Mielke
 788 et al., (2013).



789

Table 3. Summary of the average $\gamma \times f$ values derived in the field observations.

| Location | Region | $\gamma \times f$ | References |
|--------------------|----------|-------------------|-------------------------|
| Beijing, China | suburban | 0.019 | This work |
| Frankfurt, Germany | suburban | 0.014 | Phillips et al., 2016 |
| Mt. Tai, China | suburban | 0.016 | X. F. Wang et al., 2017 |
| Jinan, China | urban | <0.008 | Z. Wang et al., 2017 |
| California, USA | urban | 0.008 | Mielke et al., 2013 |

790

791

Table 4. List of the N_2O_5 uptake coefficients and the yield of CINO_2 in this campaign.

| Start time | End time | γ | f |
|-------------|-------------|----------|------|
| 05/25 00:00 | 05/25 05:00 | 0.047 | 0.60 |
| 05/25 18:30 | 05/25 23:00 | 0.012 | 1.0 |
| 05/27 19:00 | 05/27 20:40 | 0.040 | 0.50 |
| 05/28 19:00 | 05/28 23:00 | 0.017 | 1.0 |
| 05/30 21:00 | 05/31 00:00 | 0.055 | 0.55 |

792